Inorganic Chemistry

Article

pubs.acs.org/IC

In Situ Structural Characterization of Ferric Iron Dimers in Aqueous Solutions: Identification of μ-Oxo Species

Mengqiang Zhu,[†] Brendan W. Puls,[‡] Cathrine Frandsen,[§] James D. Kubicki,[‡] Hengzhong Zhang,[⊥] and Glenn A. Waychunas*,[†]

[†]Earth Sciences Division, Lawrence Berkeley National Laboratory, Berkeley, California 94720, United States

[‡]Department of Geosciences and the Earth & Environmental Systems Institute, The Pennsylvania State University, University Park, Pennsylvania 16802, United States

[§]Department of Physics, Technical University of Denmark, DK-2800 Kgs. Lyngby, Denmark

[⊥]Department of Earth and Planetary Science, University of California, Berkeley 94720, United States

Supporting Information

ABSTRACT: The structure of ferric iron (Fe^{3+}) dimers in aqueous solutions has long been debated. In this work, we have determined the dimer structure in situ in aqueous solutions using extended X-ray absorption fine structure (EXAFS) spectroscopy. An Fe K-edge EXAFS analysis of 0.2 M ferric nitrate solutions at pH 1.28−1.81 identified a Fe−Fe distance at ∼3.6 Å, strongly indicating that the dimers take the μ-oxo form. The EXAFS analysis also indicates two short Fe−O bonds at ∼1.80 Å and ten long Fe−O bonds at ∼2.08 Å, consistent with the μ-oxo dimer structure. The scattering from the Fe−Fe paths interferes destructively with that from paths belonging to $Fe(OH_2)_6^{3+}$ monomers that coexist with the dimers, leading to a less apparent Fe shell in the EXAFS Fourier transform. This might be a reason why the characteristic Fe−Fe distance was not detected in previous EXAFS studies. The existence of μ-oxo dimers is further confirmed by Mössbauer analyses of analogous quick frozen solutions. This work also explores the electronic structure and the relative stability of the μ-oxo dimer in a comparison to the dihydroxo dimer using density function theory (DFT) calculations. The identification of such dimers in aqueous solutions has important implications for iron (bio)inorganic chemistry and geochemistry, such as understanding the formation mechanisms of Fe oxyhydroxides at molecular scale.

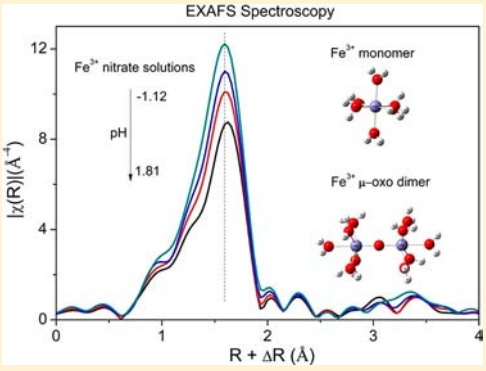

INTRODUCTION

The hydrolysis and subsequent polymerization of ferric iron (Fe^{3+}) in aqueous solutions have fundamental and environmental significance. These processes comprise the early stage formation of Fe^{3+} oxyhydroxides[1] and thus, affect dissolved Fe^{3+} speciation and phases of immediately precipitated Fe oxyhydroxides in aquatic environments.[2] However, the processes have remained largely enigmatic because of the unknown identities of polymeric Fe species.[3] Among the polymeric species, the aquo Fe^{3+} dimer is the simplest and also the only convincingly identified polymeric product,[1] but its structure has long been debated.[4−10]

Because of the difficulty of isolating the aquo dimers as crystalline salts for definitive structural determination, the early studies often inferred the dimer structure from Fe^{3+} dimer complexes involving organic chelating ligands[9,11−16] and dihydroxo, $[(H_2O)_4Fe(OH)_2Fe(H_2O)_4]^{4+}$ and μ-oxo, $[(H_2O)_5Fe(O)Fe(H_2O)_5]^{4+}$, dimers have been proposed. Later on, ion-exchanged Nafion membranes were used to isolate dimers from monomers for structural determination using extended X-ray absorption fine structure (EXAFS) and Mössbauer spectroscopy.[17,18] The results suggested a bent μ-oxo dimer structure with a Fe−Fe distance of 3.42 Å. The Mössbauer study also indicated the presence of $[(H_2O)_5Fe(H_3O_2)Fe(H_2O)_4]^{5+}$ species.[17] More direct evidence for μ-oxo dimers was provided by Junk et al.[5,6] in more recent studies where aquo dimers were isolated from Fe^{3+} nitrate and perchlorate solutions as 18-crown-6 ether (1,4,7,10,13,16-hexaoxacyclooctadecane) adduct supramolecule crystals. The X-ray diffraction (XRD)-determined structure unambiguously indicated that the dimers take the μ-oxo form.[5,6] Despite the progress made in these studies, the isolation and crystallization of dimers for structural determination are suspected to alter the dimer structure.[5,7] For instance, quantum chemical calculations suggested that the existence of μ-oxo dimers in the ether crystals might be a consequence of the crystallization process.[7] It is thus highly desirable to determine the dimer structure in situ from aqueous solution. In addition, indirect evidence from reaction kinetics and theoretical electronic structural studies advocates for the existence of the dihydroxo dimer rather than the μ-oxo form.[7,10,19,20]

Received: September 21, 2012
Published: May 23, 2013

   dx.doi.org/10.1021/ic302053w | Inorg. Chem. 2013, 52, 6788−6797

EXAFS spectroscopy is an in situ approach for determining the local atomic environment (≤6 Å) of an element of interest. Morrison et al.[21,22] used EXAFS spectroscopy to determine the structure of dimers present in 1.8 M Fe^{3+} perchlorate solution. The initial attempt by these authors indicated the dihydroxo form[22] but that conclusion has been disputed on the basis of poor data quality and erroneous data analysis.[21, 23] A later reported EXAFS spectrum on a similar solution, but of higher quality, did not exhibit obvious Fe−Fe atomic shells, and this was attributed to the low dimer abundance in the solution.[21, 23] In the present study, we have been able to enhance the dimer abundance in ferric iron nitrate solutions without leading to formation of any iron oxyhydroxide phases, which is confirmed by EXAFS, UV−vis, and Mössbauer analyses, and then used EXAFS spectroscopy to determine the dimer structure in situ. The EXAFS analysis strongly supports the existence of μ-oxo dimers rather than the dihydroxo form. The electronic and geometric structures as well as the relative stability of the two types of dimers were also computationally explored using density functional theory (DFT).

EXPERIMENTAL SECTION

Sample Preparation. All chemicals used were of analytical grade, purchased from Sigma-Aldrich. A 0.8 M (0.786 M measured by ICP-MS) ferric iron nitrate stock solution was prepared by adding 6.50 g of $Fe(NO_3)_3{\cdot}9H_2O$ crystals to 16 g of deionized (DI) water. The obtained Fe solution was used within 24 h after preparation, although it remained stable for more than a year based on its unchanged UV−vis spectrum. Three partially neutralized Fe solutions were made by adding 4 mL of DI water, 0.08 or 0.2 M $NaHCO_3$ solutions to 4 mL of 0.4 M Fe nitrate solution (2 mL of 0.8 M Fe stock solution plus 2 mL of DI water) to achieve HCO_3^- to Fe^{3+} molar ratio (represented by *h*) of 0, 0.2, and 0.5, respectively. Hereafter, they are referred to as *h0*, *h02*, and *h05*. A nitric-acid acidified Fe solution was prepared by adding 4 mL of concentrated HNO_3 to 4 mL of 0.4 M Fe nitrate solution, referred to as *ha*. Thus, the final Fe concentration of these solutions was 0.2 M. The pH of *ha*, *h0*, *h02*, and *h05* were −1.12, 1.28, 1.53, and 1.81, respectively, measured using a pH meter calibrated with pH 2, 4, and 7 buffer solutions. A reference aquo dimer compound, that is, 18-crown-6 ether adduct of μ-oxo aquo Fe^{3+} dimer (abbreviated as Fe-crown hereafter), was prepared using the procedure described in Junk et al.[6]

UV−vis Spectroscopy. UV−vis spectra were collected from the above freshly prepared solutions using the Agilent UV−vis spectrophotometer 8453. A 1-mm path length quartz cuvette was used for the measurements with DI water as the background.

XAS Data Collection and Analyses. Each of the freshly prepared solution samples was transferred to a 2-mm thick, 15-mm long, and 10-mm wide cell made from acrylic plastic. The opposing sides of the cell were sealed with Kapton film as windows. Fe K-edge EXAFS spectra were collected from each sample at one scan per 2 s in transmission mode using a quick-scan setup.[24] The spectra collected over 30 min intervals were averaged to improve counting statistics as the solution did not evolve with time based on a UV−vis check. The measurements were conducted at beamline X18B at the National Synchrotron Light Source, Brookhaven National Laboratory, using a specially equipped monochromator with a Si (111) crystal. The monochromator was detuned by 35% with respect to incident X-ray intensity (I_0) to minimize higher order harmonic X-rays. EXAFS spectra were processed using the program Athena,[25] including energy calibration using an Fe metal foil, averaging, background removal, and normalization procedures. Fourier transforms $|\chi(R)|$ were performed on k^3-weighted spectra ($k^3\chi(k)$) over a k range of 3−14 $Å^{-1}$ using the Bessel-Kaiser window. EXAFS fitting was performed using SixPack[26] to obtain the local atomic environment around the Fe atoms. Theoretical amplitude and phase shift files used for the fitting of dimers were created using Feff7[27] from the theoretical structure of a μ-oxo dimer which had been energy minimized using density functional theory (DFT) (see below).

Mössbauer Spectroscopy. To assist in identifying Fe species, Mössbauer spectroscopic analysis using frozen solutions of *h0*, *h02*, and *h05* were obtained. Each solution was quickly mixed with 50% glycerol (v/v), hand shaken, transferred to a 7-mm high cylindrical container with a 16-mm diameter, and then immediately immersed into liquid nitrogen. The solution has to be frozen to produce large effective Mössbauer recoil-free fractions and small Doppler broadening (diffusional) effects. Glycerol addition is critical for Mössbauer analysis of solution samples, as it facilitates formation of vitreous ice and thus prevents solute segregation/aggregation.[28] Numerous studies show that such intervention has minimal effects on speciation and solution equilibria. ^{57}Fe Mössbauer spectrum was collected from the frozen solutions at T = 18 K in transmission mode using constant acceleration spectrometers with sources of ^{57}Co in Rh. The spectrometers were calibrated using a 12.5 μm foil of α-Fe. The temperature was controlled using a closed-cycle helium refrigerator from APD Cryogenics. The spectrum was fitted using the program mfit. Doublet and sextet lines were constrained to be equal in width and intensity. Additionally, the relative areas of sextet lines were constrained to be 3:2:1:1:2:3.

Quantum Chemical Calculations. To assist in the interpretation of the EXAFS results, DFT calculations were used for geometry optimization (i.e., energy minimization) of a variety of Fe^{3+} monomers and dimers including $Fe(H_2O)_6^{3+}$, $Fe(OH)(H_2O)_5^{2+}$, *trans* and *cis* $Fe(OH)_2(H_2O)_4^+$, $[(H_2O)_4Fe(OH)_2Fe(H_2O)_4]^{4+}$, and $[(H_2O)_5FeOFe(H_2O)_5]^{4+}$. Fe^{3+} atoms in monomers and dimers were set in high-spin, ferromagnetic states. The method B3LYP[29,30] with the basis set 6-31G(d)[31] implemented in Gaussian 03[32] was used for the energy minimization calculations. These energy minimizations were performed in vacuum.

To compare the relative stability of the two types of dimers, their structures were reoptimized by adding two H_2O molecules, partially accounting for the second hydration shell. In addition, the ground-state antiferromagnetic (GSA) electronic configurations of the two dimers were optimized to examine their antiferromagnetic preferences using the method B3LYP with the basis set 6-31G(d) implemented in Gaussian 09.[33] Frequency calculations were performed on each minimum-energy structure and no negative frequencies were predicted indicating that a dynamically stable, minimum energy structure was obtained. (Note: We do not claim that any structure is necessarily in a global energy minimum, but the structures are at least in local energy minima.) The zero-point energy (ZPE), Gibbs free-energy (GFE), and translational energy (TE) corrections were calculated based on these gas-phase energy-minimized structures. The TE corrections were included to account for the loss of gas-phase translational entropy in the aqueous phase and were calculated based on the translational entropy of the structures at 298.15 K. The energies of the optimized structures were further refined with an implicit hydration model, the Integral Equation Formalism Polarized Continuum Model (IEFPCM),[34] to obtain the aqueous potential energies of the models (i.e., Model GFE = IEFPCM potential energy + gas-phase ZPE correction + gas-phase thermal correction − gas-phase TE correction). The refined energies were used for the stability comparison. Notably, the μ-oxo dimer contains one more H_2O molecule than the dihydroxo dimer and thus, the energy comparison is based on the dihydroxo dimer versus the μ-oxo dimer minus an isolated H_2O molecule. H_2O GFE was calculated with the same method as described above and equals −200566 kJ/mol.

RESULTS

UV−vis Spectroscopy and Fe^{3+} Species Distribution. UV−vis spectra are distinctive for Fe^{3+} monomers, molecular clusters, and particles having a periodic crystal structure. Ligand-field or d-d transitions (>400 nm) are spin forbidden and thus are extremely weak in Fe^{3+} monomers.[19,35] Antiferromagnetic coupling, increased covalence of Fe−O bonds, and intensity gain from low energy ligand−metal charge

dx.doi.org/10.1021/ic302053w | Inorg. Chem. 2013, 52, 6788−6797

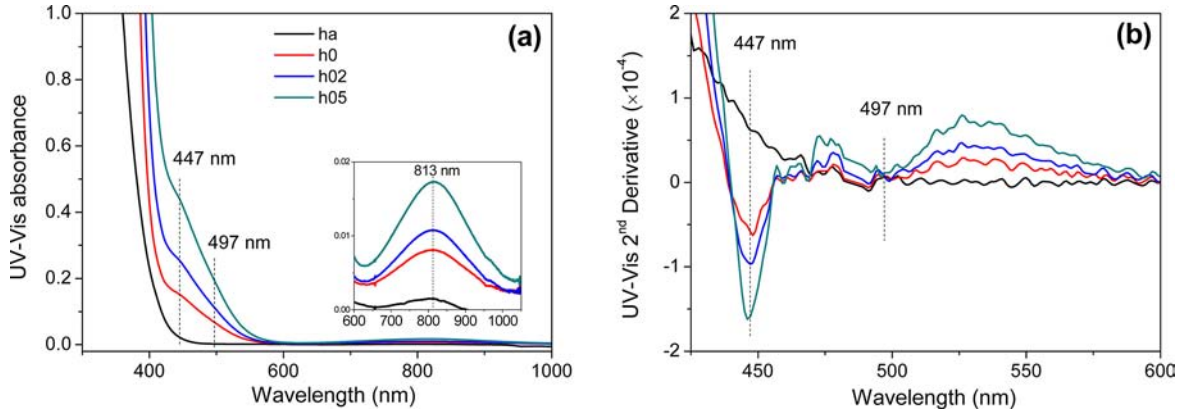

Figure 1. UV−vis spectra (a) and their 2nd derivatives (b) of 0.2 M ferric iron nitrate solutions. The low intensity bands at 813 nm are plotted in the inset. *ha* represents a HNO_3-acidified solution; *h0*, *h02*, and *h05* are solutions partially neutralized using $NaHCO_3$ at the $[HCO_3^-]/[Fe^{3+}]$ ratios of 0, 0.2, and 0.5, respectively. The spectra were measured using a quartz cuvette with a 1-mm path length. The UV−vis spectra were smoothed before calculating the derivatives. The two minima in (b) indicate the center positions of the UV−vis bands. The valleys in (b) get deeper as *h* increases, indicating increasing concentration of the Fe dimers.

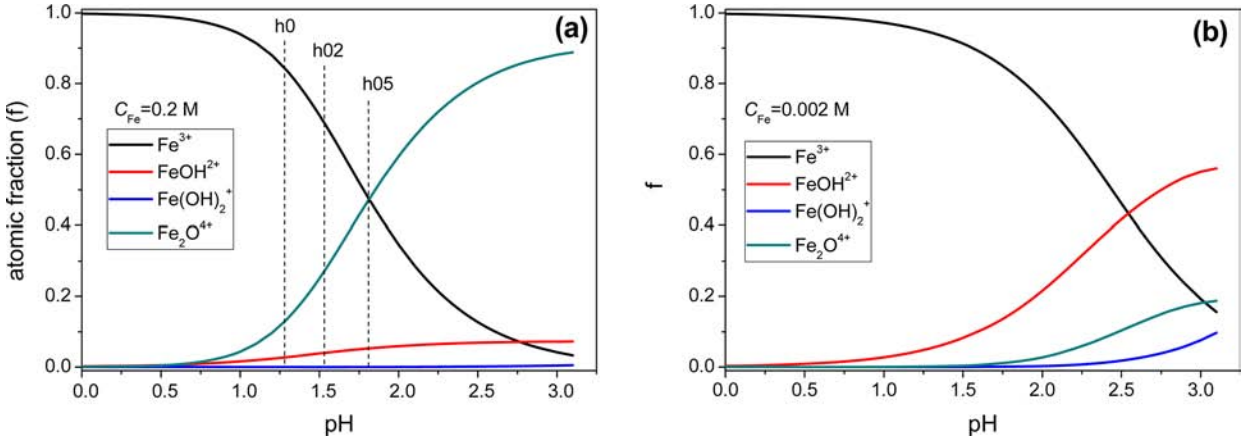

Figure 2. Fe^{3+} speciation distributions as a function of pH and total Fe concentration based on the hydrolysis constants reported by Stefansson.[50] Only the four major species were considered. Nitrate is assumed not to complex with Fe^{3+}.

transfer bands, greatly enhance the ligand-field transition probability in Fe^{3+} clusters and particles,[6,14] resulting in significant absorption bands beyond 400 nm. Fe^{3+} oxide particles also have intense electron pair transition (EPT) bands that mainly contribute to the color of Fe oxides.[36]

We used UV−vis spectroscopy to determine whether the ferric nitrate solutions contain clusters or particles. As shown in Figure 1a, the spectrum of *ha* does not have pronounced bands beyond 400 nm, indicating neither polymeric species nor particles exist but only monomers, consistent with the extreme acidity of the solution. Notably, the monomer absorption bands below 400 nm cannot be measured because of the saturation of the UV−vis detector caused by the strong Fe^{3+} ligand-to-metal transition (LMCT) absorption bands in this region and the high Fe^{3+} concentration (0.2 M).

The spectra of *h0*, *h02*, and *h05* have three absorption bands at 447, 497, and 813 nm (inset), according to second derivative calculations (Figure 1b). These bands are beyond 400 nm, indicating that Fe^{3+} clusters or Fe oxide particles form from monomers as solution pH increases. Based on the fact that Fe oxides do not have bands around 800 nm (except for hematite),[36] the presence of the 813 nm band suggests that the Fe species is not Fe oxide. Although the 497 nm band resembles the EPT band, the band has much weaker intensity than the EPT band at ~485 nm observed in our previous study,[37] in which ferrihydrite and schwertmannite formed in solutions. Therefore, we conclude that the three bands result from Fe^{3+} molecular clusters rather than Fe oxide particles. From *h0* to *h05*, the band positions do not change whereas their absorbance increases to the same extent (Supporting Information, SI-1), indicating that all three bands result entirely from a single type of Fe cluster whose abundance increases with increasing pH.

According to the Fe^{3+} species distribution as a function of pH (calculation details in Supporting Information, SI-2), shown in Figure 2a for C_{Fe} = 0.2 M, dimers and hydrated Fe^{3+} monomers ($Fe(H_2O)_6^{3+}$) dominate the distribution with minor $Fe(OH)(H_2O)_5^{2+}$. Dimer atomic fractions increase with pH and the fractions in the *h0*, *h02*, and *h05* solutions are 0.13, 0.27, and 0.47, respectively. These fractions linearly correlate with the UV−vis absorbance at 447 and 813 nm (Supporting Information, SI-1), indicating that the Fe molecular cluster observed by UV−vis spectroscopy is actually a dimer. Based on the linear relationship, the UV−vis absorbance coefficients for dimers can be estimated as 44.6 ± 0.8 $mol{\cdot}L^{-1}cm^{-1}$ for the 447 nm band and 1.15 ± 0.04 $mol{\cdot}L^{-1}cm^{-1}$ for the 813 nm band.

Although these solutions (*h0*, *h02*, and *h05*) are saturated with respect to Fe^{3+} oxyhydroxide phases,[23] aging of the

dx.doi.org/10.1021/ic302053w | Inorg. Chem. 2013, 52, 6788−6797

solutions for one day did not change the UV−vis spectra, suggesting relative stability of the Fe dimers. However, aging of *h*05 over 4 days at room temperature did lead to particle formation, indicated by appearance of an intense EPT band at ∼488 nm[37] (data not shown).

EXAFS Spectroscopy. EXAFS analysis was employed to determine the local atomic structure around Fe atoms and infer the structure of the Fe dimers. Figure 3 shows the Fe K-edge EXAFS (Figure 3a) and their Fourier transforms (Figure 3b) for the solution samples. The intense peaks at ∼1.6 Å (R+ΔR) correspond to the nearest O shells at ∼2.0 Å from the central Fe (Figure 3b), that is, the Fe−O bond lengths. From *ha* to *h05*, the peaks decrease dramatically in height but increase in width; the positions of the peak maxima shift to the right and meanwhile, a peak shoulder at ∼1.25 Å (R+ΔR) gradually develops (indicated by the arrow). These observations suggest splitting of the Fe−O bond lengths, that is, some shortened and others elongated with increasing pH. Consequently, EXAFS backscattered waves from the two split O subshells can interfere destructively with each other, producing the decreasing peak heights in the Fourier transforms[37]

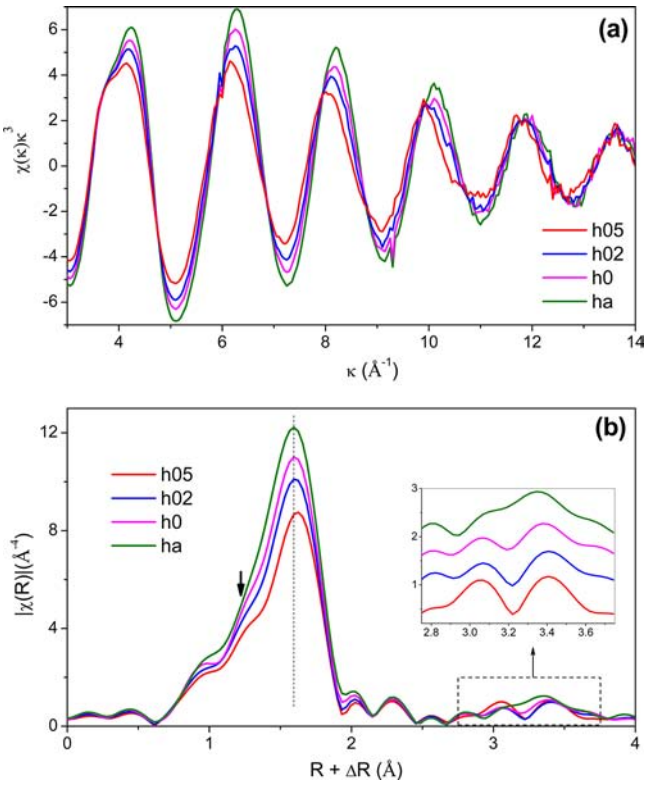

Figure 3. k^3-weighted Fe K-edge EXAFS spectra and their Fourier transform magnitude for partially neutralized 0.2 M Fe^{3+} nitrate solutions. The inset shows the expanded view with vertical offsets of 2.75−3.75 Å regime for a clearer visualization. The bold arrow indicates that a shoulder develops as the neutralization degree increases.

The Fe atomic shell in the edge-sharing Fe moiety is usually located at 2.5−2.7 Å (R+ΔR), corresponding to an Fe−Fe distance at ∼2.9−3.1 Å, such as in ferrihydrite and schwertmannite.[37] However, Figure 3 shows that the peak amplitude in this regime is very weak and changes negligibly from *ha* to *h05*, indicating that the Fe species in these solutions do not have the edge-sharing moiety or the abundance of this moiety is too low to be detected by EXAFS spectroscopy. This rules out significant concentrations of the dihydroxo dimers and iron oxyhydroxide particles because the edge-sharing moiety is their essential structural unit.

In contrast, pronounced peaks exist at 2.75−3.75 Å (R+ΔR) and change significantly from *ha* to *h05*. The solution *ha* must not contain an appreciable amount of clusters because of its extreme acidity. The peaks of *ha* at larger R values are attributed to both single-scattering (SS) paths from the O atoms in the second hydration shell and the multiple-scattering (MS) paths within the first hydration shell.[38] The differences between *ha* and the other three solutions in the high R region suggest the presence of additional scattering paths. This can be discriminated by curve fitting of the EXAFS spectra, as shown below.

The EXAFS fitting was performed over 1−3.8 Å (R+ΔR) in R space, covering the major peaks. The O peak at 1.6 Å (R +ΔR) of sample *ha* is asymmetric, indicating an anharmonic effect, and can be fitted well using a single O shell including the use of the third cumulant.[39] Fitting of the R peaks at 2.75−3.75 Å (R+ΔR) suggests the necessity to include both MS paths within the first hydration shell and the SS Fe−O path from the

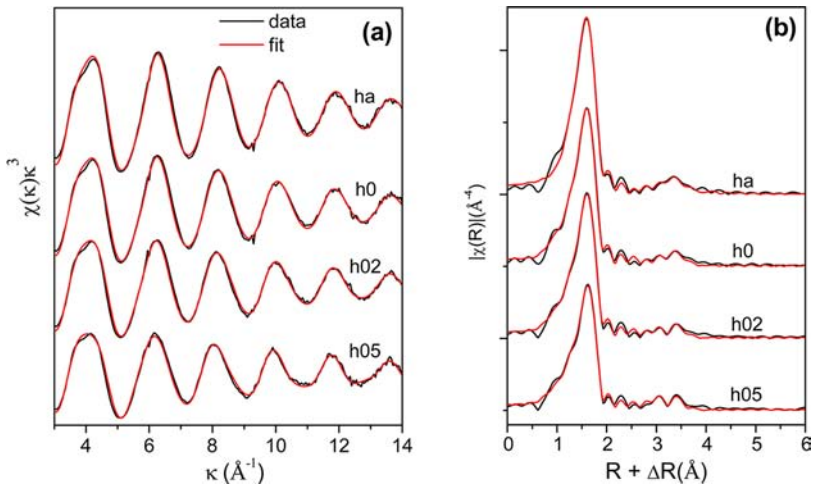

Figure 4. EXAFS data (black) and fits (red) for partially neutralized ferric Fe nitrate solutions: k^3-weighted spectra (a) and their Fourier transform magnitudes (b).

dx.doi.org/10.1021/ic302053w | *Inorg. Chem.* 2013, 52, 6788−6797

second hydration shell. The coordination number (CN) of the second hydration shell was fixed at 12, and its path length and Debye–Waller factors (σ^2) were floated. All four types of MS paths were used in the fitting, and their path lengths and σ^2 were parametrized using those belonging to the Fe–O SS path.[38] The CNs of these MS paths were fixed at the theoretical values. Therefore, the inclusion of the MS paths does not introduce any additional fitting parameters. As such, there are a total of 7 free parameters (including ΔE and S_0) in the fit, which are much fewer than 18 independent parameters (degrees of freedom) permissible given the ΔR backtransfrom window width and the EXAFS Δk value. The theoretical phase and amplitude files used for the paths in the fitting were created from a FeO_6 octahedron using Feff7. It can be seen that the fit agrees well with the data (Figure 4). The obtained parameters are listed in Table 1, labeled as "Monomer" considering that it is the only Fe species in this solution (*ha*). The obtained Fe–O distances in the first and second hydration shells are 1.989 ± 0.006 Å and 4.31 ± 0.06 Å, respectively (Table 1). Note that σ^2 (0.03 ± 0.01) is quite large for the Fe–O_{hyd} path.

Table 1. EXAFS Shell-by-Shell Fitting Results for Ferric Fe Nitrate Solutions

	shell	[c]CN	d (Å)	σ^2
[a]monomer	Fe–O	6	1.989(6)	0.005(1)
	[d]Fe–O_{hyd}	12	4.31(6)	0.03(1)
[b]dimer	Fe–O_1	1	1.806(7)	0.004(2)
	Fe–O_2	5	2.07(1)	0.005(1)
	Fe–Fe	1	[e]3.61	*0.002(1)*
	$FeOFe_{MS}$	2	[e]3.61	*0.02(1)*

samples	R	Red-χ^2	[f]$f_{monomer}$	f_{dimer}	ΔE(eV)
acidified (*ha*)	0.0049	44.1	1	0	−5.1(3)
h = 0 (*h0*)	0.0038	23.7	0.90	0.10(3)	−5.2(3)
h = 0.2 (*h02*)	0.0041	30.3	0.80	0.20(2)	−5.3(3)
h = 0.5 (*h05*)	0.0043	33.0	0.63	0.37(7)	−5.1(4)

[a]The monomer parameters were obtained by fitting the EXAFS spectrum of an acidified iron nitrate solution (*ha*). The third cumulant expansion term C_3 was used for the fit of the first O shell and was determined to be −0.0015(7). All multiple scattering (MS) paths within the 1st hydration shell were included as well as the single scattering (SS) path from the 2nd hydration shell (Fe–O_{hyd}). [b]The dimer parameters were obtained by fitting the spectrum of the h = 0.5 solution (*h05*). The monomer parameters were fixed as those of *ha*, and the dimer parameters, its atomic fractions (f_{dimer}) and ΔE were allowed to float in the fitting. The parameters obtained for both monomer and dimer as above were fixed in the fitting for the h = 0 (*h0*) and h = 0.2 (*h02*) solutions, and only f_{dimer} and ΔE values were refined. [c]CNs were fixed as the theoretical values. [d]The 2nd hydration shell. [e]The path lengths were correlated with R_{Fe-O1} as $2*R_{Fe-O1}$. [f]The atomic fractions of monomer, $f_{monomer} = 1 - f_{dimer}$.

However, the above fitting model cannot fit well the spectra of the partially neutralized samples (*h0*, *h02*, and *h05*), particularly for the R peaks at 2.5–2.7 Å (R+ΔR), which suggests the presence of dimers. To fit these spectra, the following fitting model was developed based on the structure of μ-oxo dimer since the possibility for the dihydroxo dimer had been excluded based on the qualitative analysis. The solutions contain predominantly aquo monomers and dimers, with a minor additional content of $Fe(OH)(H_2O)_5^{2+}$ according to the Fe species distribution (Figure 2a). This result is also consistent with EXAFS principal component analysis that indicates only two major Fe species existing in these solutions (Supporting Information, SI-3). Hence two separate sets of fitting parameters were used for hydrated monomers and dimers, respectively, and the presence of $Fe(OH)(H_2O)_5^{2+}$ was neglected. We assume that the hydrated monomer and its second hydration shell in these solutions are identical to those in sample *ha*. Then the monomer parameters from *ha* were fixed in the fits for *h0*, *h02*, and *h05* and only its atomic fractions ($f_{monomer}$) were allowed to vary. As for the dimer, its parameters were refined as well as its atomic fraction that was defined as $f_{dimer} = 1 - f_{monomer}$. The detailed fitting model is described below.

According to the μ-oxo dimer structure reported by Junk et al.,[6] the bond length (1.784 Å) between Fe and the μ-oxo O is 0.265–0.339 Å shorter than the other five Fe–OH_2 bonds (2.049–2.123 Å).[6] Such length difference is larger than the permissible resolution ($\Delta R = \pi/(2\Delta k)$ = 0.14 Å) expected for the data ranges analyzed. Thus, two separate O subshells can be used in the fits, one accounting for μ-oxo O (CN = 1) and the other for the five H_2O (CN = 5). In addition to the Fe–Fe SS path between the two Fe centers in the μ-oxo dimer, several MS paths associated with the Fe–O–Fe moiety were identified based on the Feff calculation of the DFT-optimized μ-oxo dimer, but including only the following type is found to be sufficient for a good fit. This path has the largest amplitude contribution among all Fe–O–Fe MS paths according to the Feff calculation.The path lengths for both Fe–Fe SS and

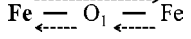

FeOFe MS paths are defined as $2*R_{Fe-O1}$, assuming the Fe–O_1–Fe moiety has a linear structure. Their Debye–Waller factors also are assumed to be uncorrelated. The CNs of the Fe–Fe SS and the FeOFe MS paths were fixed at theoretical values 1 and 2, respectively. Additionally, several MS paths exist within the first hydration shell of the Fe in the dimer. However, we believe these MS paths are not important contributors to the EXAFS amplitude because the MS paths tend to interfere destructively with each other[40] because of the varying lengths of Fe–OH_2 bonds[6] and the large kinetic labilities of these bonds.[40,41] The varying lengths would also be expected to result in a more disordered second hydration shell. Hence, the second hydration shell was not considered in the dimer fit.

According to the species distribution (Figure 2a), the *h05* solution contains the most abundant dimers and hence has a larger EXAFS contribution from dimers than the other two solutions. Therefore, the fitting was started with this sample for a more reliable assessment of the dimer parameters. The determined parameters for the dimer as such are listed in Table 1. Then these dimer parameters were again fixed in the fits for *h0* and *h02* and only the atomic fractions were refined. Comparisons between spectra and the fits are given in Figure 4. Good agreements are achieved based on both visual inspections (Figure 4) and statistical analyses (R and red-χ^2 values in Table 1). The obtained Fe–O bond lengths are 1.806 ± 0.007 Å and 2.07 ± 0.01 Å, and the dimer atomic fractions are 0.10 ± 0.03, 0.20 ± 0.02, and 0.37 ± 0.07, respectively, for *h0*, *h02*, and *h05*.

Mössbauer Spectroscopy. The 18 K spectra of the vitrified *h0*, *h02*, and *h05* solutions all contain a magnetically split component (S_a) attributed to Fe^{3+} monomers with slow paramagnetic relaxation (Figure 5). Such components cannot be described fully in terms of sextets, and fitting of such components is extremely complex.[42,43] Only if a large magnetic field is applied can the spectrum be described as a sum of sextet

dx.doi.org/10.1021/ic302053w | Inorg. Chem. 2013, 52, 6788–6797

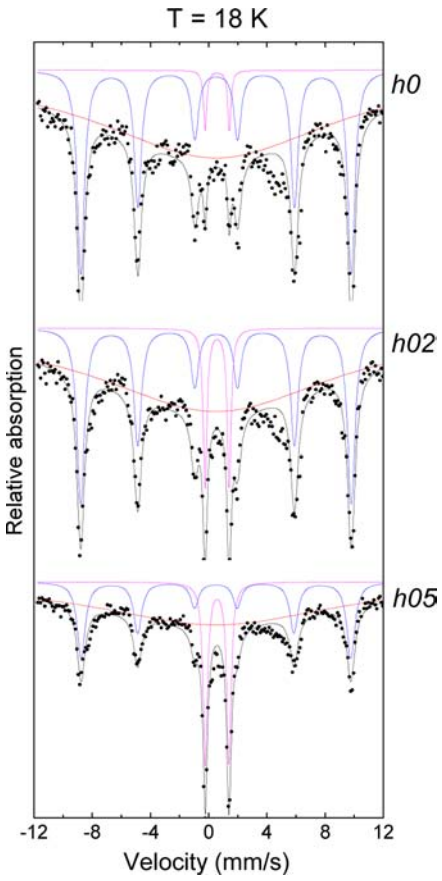

Figure 5. Mössbauer spectra (dots) and the fits (lines) of the frozen *h* = 0, 0.2, and 0.5 solutions. The doublets have isomer shifts of ∼0.59 mm/s and quadrupole splitting of about ∼1.65 mm/s. The sextets have isomer shifts of ∼0.50 mm/s and hyperfine fields of ∼56.7 T (Bhf). In addition, singlets with isomer shifts of ∼0.49 mm/s have to be added to account for species with magnetic relaxation time on the order of a few nanoseconds, especially from monomeric species. The parameters are listed in the Supporting Information.

components.[43−45] To obtain an approximate estimate of the Mössbauer parameters of the monomer component, we fitted with one sextet S_a with magnetic hyperfine field of ∼57.6 T, with an isomer shift of ∼0.50 mm/s and zero quadrupole shift (Table S1 in Supporting Information, SI-4). These parameters correspond to the $Fe(H_2O)_6^{3+}$ complex.[43−45] A broad singlet is added to the fits to account for species (mainly monomers) with relaxation times of around a few nanoseconds. In addition, the spectra all contain a ferric doublet (D_a) with an isomer shift (δ) of ∼0.58 mm/s and quadrupole splitting (ΔE_Q) of ∼1.65 mm/s. These values are very close to those of the [18]crown-6 ether aquo μ-oxo dimer crystals[6] which have a δ of 0.52 mm/s and ΔE_Q of 1.69 mm/s at 77 K. This strongly indicates that the doublets of these solutions correspond to the μ-oxo dimer rather than Fe^{3+} oxides and oxyhydroxides that have distinct Mössbauer parameters. The strong quadrupole splitting of ∼1.65 mm/s is also consistent with the strong Fe−O covalent bonds in the μ-oxo dimer, ruling out the possibility of the dimer being the dihydroxo form. With increasing neutralization from *h0* to *h05* (Figure 5) the spectra show an increase in dimer abundance (Supporting Information, Table S1). An assignment to μ-oxo dimers has also been made in a previous Mössbauer study by Knudsen et al.[42] In their study, μ-oxo dimers were identified to be the only condensed species in ferric perchlorate solutions of $h \leq 0.5$.[42]

Quantum Chemical Calculations. DFT energy minimizations were performed on those Fe monomer and dimer structures possibly present in aqueous solutions. The obtained geometrical parameters are shown in Figure 6 and the molecular images are given in Figure 7 for the dimers and in the Supporting Information (SI-5) for the rest. All six Fe−OH_2 bonds in $Fe(H_2O)_6^{3+}$ are the same at 2.04 Å while the Fe−O bond lengths split in the hydrolyzed species, that is, Fe−OH bonds shortened and Fe−OH_2 bond elongated, because of the "conjugate base" labilization effect.[46−48] As for the μ-oxo dimer, the two Fe-OFe distances are quite short (1.84 Å). All ten Fe−OH_2 bonds in the μ-oxo dimer are elongated because of the labilization effect[46−48] but the two at *trans* positions are much longer (2.21 Å) than those equatorial Fe−OH_2 bonds (2.07 and 2.11 Å), indicating an additional *trans* effect.[49] The Fe−Fe distance in the μ-oxo dimer is 3.68 Å and the Fe−O−Fe angle is 180.0°. As for the dihydroxo dimer, Fe−O bond lengths in Fe−OH and Fe−OH_2 ranged from 1.95 to 2.09 Å, less splitting than observed in the μ-oxo dimer. The predicted Fe−Fe distance in the dihydroxo dimer is 3.19 Å.

The Gibbs free energy (GFE) differences (ΔG) and structures of the two dimers reoptimized with two additional H_2O molecules are shown in Figure 7. The GFE for each dimer species can be found in the Supporting Information (SI-6). Including the second water shell and subtracting the extra H_2O molecules results in an energy reduction of −60 kJ/mol for the dihydroxo dimer and −79 kJ/mol for the μ-oxo dimer; this is essentially the H-bond energy between the H_2O and the dimers. The energy comparison indicates that when the additional H_2O molecules are absent, the μ-oxo dimer is preferred thermodynamically to the dihydroxo dimer by an energy difference of −5 kJ/mol. When the stabilizing H_2O molecules were added, the μ-oxo dimer is preferred thermodynamically to the dihydroxo dimer by an energy difference of −23 kJ/mol, suggesting the importance of the second shell hydration in further stabilizing the μ-oxo dimer.

The optimization of the GSA electronic configurations for both the first hydration shell and the stability-enhanced models of the dihydroxo dimer converged successfully but resulted in negligibly higher energies than the ferromagnetic configurations. This suggests that both spin states can coexist. The optimization of the GSA electronic configurations for both the first hydration shell and the stability-enhanced models of the μ-oxo dimer failed to maintain their spin-ordering and converge to a stable minimum; however, the unconverged energies are higher by 387 and 388 kJ/mol, respectively, than their ferromagnetic analogues. Therefore, we conclude that GSA spin-ordering has an insignificant effect on the energies for the dihydroxo dimers and is higher in energy than the ferromagnetic state for the μ-oxo dimer.

DISCUSSION

Six soluble Fe species can exist in the solutions, including the five hydrated and hydrolyzed monomers $Fe(H_2O)_m(OH)_n^{3-n}$ (n = 0−4, $m + n = 6$) and one dimer.[50] The relative abundances of these soluble species are highly dependent on solution pH and total Fe^{3+} concentration.[51] The successful structural determination of dimers in this study is attributed to the use of appropriate pHs and Fe concentrations producing abundant dimers (Figure 2), but meanwhile not leading to observable particle formation, as indicated by the EXAFS, UV−vis, and

dx.doi.org/10.1021/ic302053w | Inorg. Chem. 2013, 52, 6788−6797

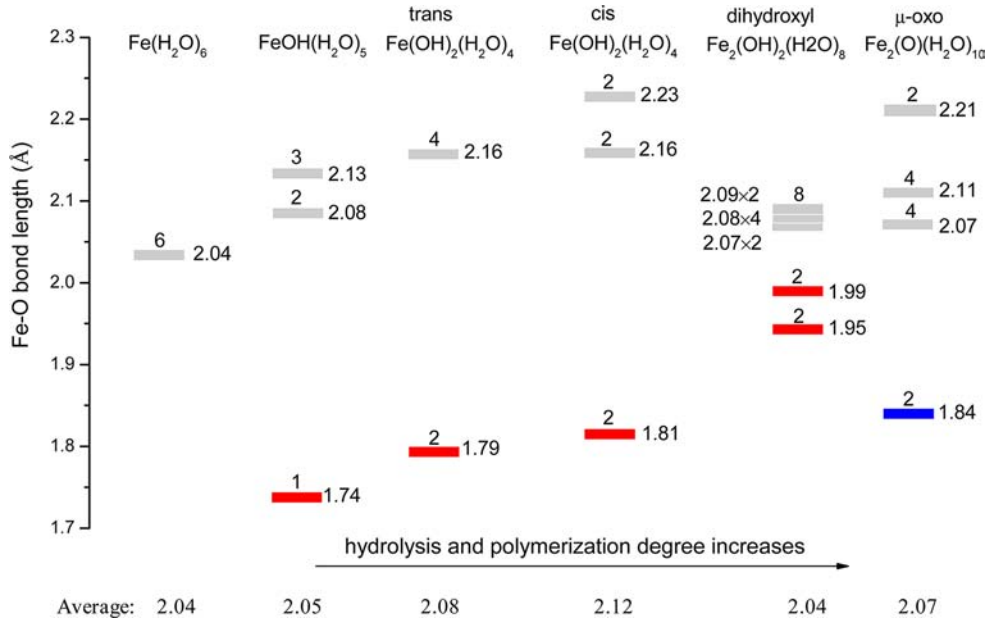

Figure 6. Fe−O bond lengths in angstrom (Å) in DFT-optimized ferric iron monomers and dimers. Gray, red, and blue bars indicate Fe−OH_2, Fe−OH, and Fe−OFe bonds, respectively. The numbers above the bars are numbers of bonds, and the values besides bars are bond lengths. The numbers at the bottom are the average values of the Fe−O bond length for each species. The monomer group includes $Fe(H_2O)_6^{3+}$, $Fe(OH)(H_2O)_5^{2+}$, and *trans* and *cis* $Fe(OH)_2(H_2O)_4^{+}$. The dimer group includes the dihydroxo and μ-oxo dimers. From left to right, the Fe^{3+} hydrolysis and polymerization degree increases.

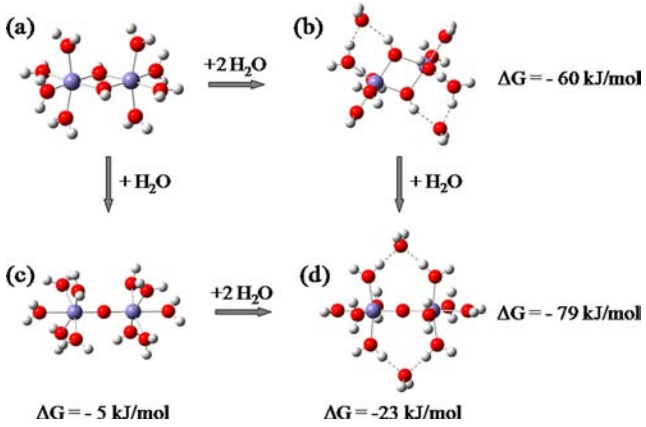

Figure 7. Structures of the dihydroxo (a, b) and μ-oxo (c, d) dimers with only their 1st hydration shells (a, c) and two additional H_2O molecules (b, d). The Gibbs free energy (GFE) differences (ΔG) were calculated for each reaction constructed based on the stoichiometric relations between the dimers (i.e., the GFEs of two isolated H_2O molecules were subtracted from b and d when calculating the ΔGs from steps a to b and c to d, and the GFE of one isolated H_2O molecule was subtracted from c and d when calculating the ΔGs from steps a to c and b to d). The calculated GFE for each dimer species is provided in the Supporting Information.

Mössbauer results. The solution conditions also suppress the formation of hydrolyzed monomers, making dimers and $Fe(H_2O)_6^{3+}$ the dominant species (Figure 2), and accordingly simplifying the EXAFS analysis.

The Fe−OH_2 bond length of 1.989 ± 0.006 Å in the acidified solution (*ha*) is in excellent agreement with 1.98−1.99 Å reported in previous EXAFS studies[52,53] but slightly shorter than the diffraction-determined values,[54,55] which could be due to the anharmonicity of the scattering paths. As to the second hydration shell, however, its distance from the center Fe (4.31 ± 0.06 Å) is 0.2 Å further than those determined by the diffraction measurements.[54,55] The difference may be ascribed to systematic errors of the two methods and the dynamic disordering in the second hydration shell, indicated by the large σ^2 value.[40] As for the μ-oxo dimer, the determined Fe−O bond lengths (1.806 ± 0.007 Å and 2.07 ± 0.01 Å) agree well with those bond lengths in the Fe-crown ether sample[6] which were 1.784 Å for Fe−O_{oxo} and 2.08 Å for an average of the five Fe−OH_2 bonds. The Fe−O bond length in the monomer sits between the two Fe−O bond lengths from the dimer, leading to the shift of the O peak maxima to longer R values and an emerging shoulder on the left side of the peak, as the dimer abundances increase and the monomer abundances decrease from *h0* to *h05*. The relative abundance changes of monomers and dimers also alter the XANES and pre-edge features (see detailed discussion in the Supporting Information, SI-7).

The atomic fractions of the dimers in the three solutions were quantified using the EXAFS shell-by-shell fitting. To check if the EXAFS quantification is consistent with other estimates, the f_{dimer} values are compared with the fraction values calculated in the species distribution. A good linear relationship is obtained although the shell-fitting-determined f_{dimer} are smaller by 20−25% than those in the species distribution (Supporting Information, SI-8). However, the deviation is acceptable considering relatively large uncertainties in Feff-calculated path scattering amplitude which is manifested with the 20% error in the determination of CNs using EXAFS spectroscopy. In addition, the neglect of the $Fe(OH)(H_2O)_5^{2+}$ in the fitting model may also contribute to the deviation.

Our high quality spectra and consistency between the multiple analyses ensure that the relatively weak larger R peaks in the EXAFS Fourier transforms are real scattering contributions rather than some type of noise contributions or Fourier ripples associated with the Fe−O peak or because of improper handling of the Fourier transform and windowing

dx.doi.org/10.1021/ic302053w | *Inorg. Chem.* 2013, 52, 6788−6797

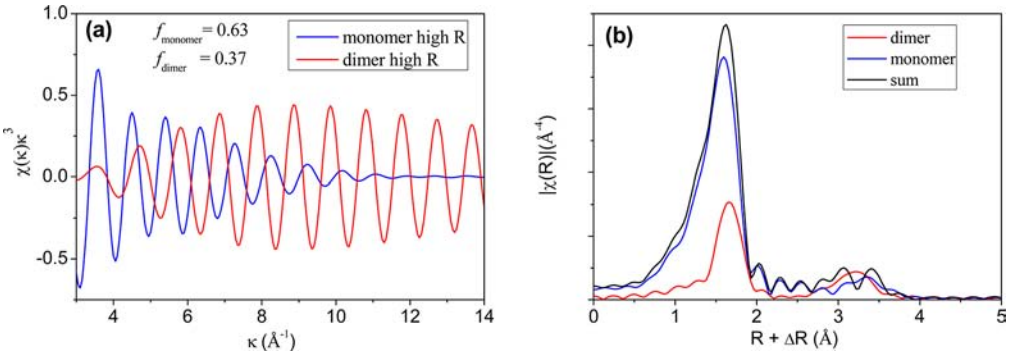

Figure 8. Respective scattering path sum for the monomer and the μ-oxo dimer used for the fitting of the high R region for the h = 0.5 solution (a), and the respective Fourier transforms for the monomer and the dimer and their sum (b). In high R regions, the scattering paths from the monomer interfere destructively, although incompletely, with the dimer scattering paths (a), leading to a disappearance of the dimer characteristic Fe peak at 3.14 Å (R+ΔR) in the Fourier transform (b).

operations. Prior to the phase correction, the sum of the Fe SS path and the FeOFe MS path should correspond to a strong peak at 3.14 Å (R+ΔR) in the Fourier transform (Figure 8b). However, destructive interference from the scattering paths associated with Fe monomers alters the appearance of the 3.14 Å (R+ΔR) peak (Figure 8a). This is likely an important reason why the μ-oxo dimer was not discovered in solutions in previous EXAFS studies.[21,56]

It is noteworthy to emphasize again here that the changes in the high R region of the Fourier transforms are not caused by any potential destructive interference between monomers and Fe oxyhydroxides. This is evident by a linear combination fitting analysis of the spectra of *h0*, *h02*, and *h05* with the spectrum of *ha* (containing monomers only) and the spectra of Fe oxyhydroxide phases including either ferrihydrite, goethite, lepidocrocite, or hematite (Supporting Information, SI-9). The results clearly show that none of the combinations represents well the EXAFS spectra of the three solution samples in both k space and the Fourier Transforms, indicating that the high R region of the Fourier transforms is not due to the destructive interferences from Fe oxyhydroxide phases. In addition, the Fe−O peaks in the Fourier transforms are also significantly different between the linear combination fits and the solution spectra, providing additional evidence that the mixtures of monomers and Fe oxyhydroxides cannot represent the Fe species in these solutions.

Although both Fe-crown and the solutions contain μ-oxo dimers, the dimers in these two different environments are not precisely identical, and this is indicated by the differences in UV−vis band positions. Three bands can be identified at ∼432, ∼ 493, and 800 nm in the diffuse reflectance UV−vis spectrum of the Fe-crown crystal reported in Junk et al.[5] (see the electronic Supporting Information in their study). These bands show blue shifts compared to the analogous bands in our study which were measured using the absorption mode in aqueous water solutions (Figure 2). The bands are essentially the same, and their wavelength differences could be due to the slight structural modifications of, for example, Fe−O bond lengths and Fe−O−Fe angle, when crystallized as solids. Thus, the 447 and 497 nm bands can be assigned to the weak O_{oxo}-Fe charge transfer and $^6A_1 \rightarrow (^4A_1, ^4E)$ and the 813 nm band to $^6A_1 \rightarrow {}^4T_1$.[5,57,58] This structural difference between the solution dimer and the crystallized analogue may also cause the observed slight discrepancy of their Mössbauer parameters.

The geometry of the dimer predicted by the DFT calculations agrees reasonably well with the EXAFS result in this study, and is also in line with those in a previous DFT study by Panina et al.[7] Regarding the dimer thermodynamic stability, DFT predicts that the μ-oxo dimer is more stable than the dihydroxo dimer. This result is consistent with our EXAFS analysis. However, Panina et al.[7] predicted a reverse order, which is probably due to improvements made to the polarized continuum model for solvation of Tomasi and co-workers.[28] In addition, the stabilization effect of the two H_2O molecules on the μ-oxo dimer is ascribed to the hydrogen bonding between H_2O molecules within the first and second shells. 18-crown-6 ether may play the same role as the second shell water molecules by providing additional hydrogen bonding and stabilizing the μ-oxo dimer in the 18-crown crystals.[6] Because there is no thermodynamic data on these species to verify our calculated energies, we rely on the fact that the μ-oxo dimer reproduces the observed EXAFS results more accurately than the dihydroxo dimer as the basis for concluding the former is more thermodynamically stable as calculated in this study.

The *trans* effect in the μ-oxo dimer destabilizes the H_2O ligand at the *trans* position, making binding of another Fe at this position less favorable. This implies that the Fe−O−Fe moiety is not able to polymerize into a longer linear chain structure in aqueous solution, for example, −Fe−O−Fe−O−Fe−O−Fe−. The linear Fe−O−Fe moiety in the μ-oxo dimer is not a structural unit of ferric iron oxyhydroxides; therefore, the presence of such dimers implies that either Fe oxyhydroxide precipitation pathways do not proceed from such units or that the dimers have to rearrange their structure to be involved in the precipitation process.

The formation of the μ-oxo dimer may involve the dihydroxo dimer as an intermediate followed by an internal dehydration between the two doubly bridged OH groups.[59] Alternatively, it may form single μ-hydroxo (μ-OH) bridged dimers first, such as $[(H_2O)_5Fe{-}OH{-}Fe(H_2O)_5]^{5+}$ or $[(H_2O)_5Fe{-}H_3O_2{-}Fe{-}(H_2O)_4]^{5+}$, and then the −OH− may undergo hydrolysis. Both pathways involve the hydrolysis step of the bridging OH groups. The preference of the μ-oxo form to the dihydroxo form suggests that Fe−OH hydrolysis occurs readily. In contrast to Fe^{3+}, both Cr^{3+} and Al^{3+} prefer dihydroxo dimers to μ-oxo dimers.[60] The difference can be due to the higher electronegativity of Fe^{3+} than those of Cr^{3+} and Al^{3+},[61] which facilitates Fe^{3+} hydrolysis.

dx.doi.org/10.1021/ic302053w | *Inorg. Chem.* 2013, 52, 6788−6797

CONCLUSION

Both dihydroxo and μ-oxo dimers have been proposed. Previous structural characterizations were conducted only ex situ, that is, crystallizing or isolating dimers prior to structural analysis, with enhanced probability that the separated dimers may not possess the same structure as those in solution. In this study, the structure of dimers in ferric iron nitrate solutions ($[Fe^{3+}]$ = 0.2 M and pH = 1.28−1.81) has been quantified using in situ EXAFS spectroscopy, corroborated by the Mössbauer analysis, and DFT calculations. The results indicate that the clusters are Fe^{3+} aquo μ-oxo dimers probably with a linear Fe−O−Fe moiety. This is the first time that the structure of aquo dimers has been successfully determined in situ in aqueous solutions, solving the long standing debate. The identification of μ-oxo dimers in acidic solutions with nonbinding nitrate ions provides a foundation for understanding ferric Fe speciation in natural acid mine drainage solutions that are enriched with sulfate ligands that can strongly bind with Fe oxyhydroxide polymers.

ASSOCIATED CONTENT

Supporting Information

EXAFS principal component analysis and linear combination fitting, the details for ferric iron speciation distribution calculation, the linear relationships between dimer quantities obtained using different analysis, XANES and pre-edge peak fitting results, Mössbauer parameters, Gibbs free energies, and monomer molecular images. This material is available free of charge via the Internet at http://pubs.acs.org.

AUTHOR INFORMATION

Corresponding Author

*E-mail: GAWaychunas@lbl.gov. Phone: + 1 510 495-2748. Fax: +1 510 486-5686.

Notes

The authors declare no competing financial interest.

ACKNOWLEDGMENTS

The work was supported by the U.S. Department of Energy, Office of Basic Energy Sciences, under Award Number DE-AC02-05CH11231 to Lawrence Berkeley National laboratory. B.W.P. and J.D.K. acknowledge support from the National Science Foundation (NSF) Collaborative Research in Chemistry grant "Structure and properties of disordered iron-oxyhydroxides" (CHE-0714121). Computational support was provided by the Research Computing and Cyberinfrastructure group at The Pennsylvania State University. C.F. acknowledges funding from The Danish Councils for Independent Research. The authors are grateful to Dr. Syed Khalid for his assistance during data collection at beamline X18B at the National Synchrotron Light Source, Brookhaven National Laboratory. Use of the National Synchrotron Light Source, Brookhaven National Laboratory, was supported by the U.S. DOE Office of Science, Office of Basic Energy Sciences, under Contract No. DE-AC02-98CH10886. Portions of this research were carried out at the Stanford Synchrotron Radiation Laboratory, a national user facility operated by Stanford University on behalf of the U.S. Department of Energy, Office of Basic Energy Sciences.

REFERENCES

(1) Flynn, C. M. *Chem. Rev.* **1984**, *84*, 31−41.
(2) Mudashiru, L. K.; Aplin, A. C.; Horrocks, B. R. *Anal. Methods* **2011**, *3*, 927−936.
(3) Rose, A. L.; Waite, T. D. *Geochim. Cosmochim. Acta* **2007**, *71*, 5605−5619.
(4) Kurtz, D. M. *Chem. Rev.* **1990**, *90*, 585−606.
(5) Junk, P. C.; McCool, B. J.; Moubaraki, B.; Murray, K. S.; Spiccia, L.; Cashion, J. D.; Steed, J. W. *J. Chem. Soc., Dalton Trans.* **2002**, 1024−1029.
(6) Junk, P. C.; McCool, B. J.; Moubaraki, B.; Murray, K. S.; Spiccia, L. *Angew. Chem., Int. Ed.* **1999**, *38*, 2224−2226.
(7) Panina, N. S.; Belyaev, A. N.; Eremin, A. V.; Davidovich, P. B. *Russ. J. Inorg. Chem.* **2010**, *80*, 889−894.
(8) Baev, A.; Evsei, E. *Russ. J. Inorg. Chem.* **2010**, *55*, 508−522.
(9) Thich, J. A.; Ou, C. C.; Powers, D.; Vasiliou, B.; Mastropaolo, D.; Potenza, J. A.; Schugar, H. J. *J. Am. Chem. Soc.* **1976**, *98*, 1425−1433.
(10) Lente, G.; Fabian, I. *Inorg. Chem.* **1998**, *38*, 603−605.
(11) Schugar, H. J.; Walling, C.; Jones, R. B.; Gray, H. B. *J. Am. Chem. Soc.* **1967**, *89*, 3712−3720.
(12) Schugar, H. J.; Rossman, G. R.; Thibeault, J.; Gray, H. B. *Chem. Phys. Lett.* **1970**, *6*, 26−28.
(13) Elam, W. T.; Stern, E. A.; McCallum, J. D.; Sanders-Loehr, J. *J. Am. Chem. Soc.* **1982**, *104*, 6369−6373.
(14) Brown, C. A.; Remar, G. J.; Musselman, R. L.; Solomon, E. I. *Inorg. Chem.* **1995**, *34*, 688−717.
(15) Schugar, H.; Rossman, G. R.; Gray, H. B. *J. Am. Chem. Soc.* **1969**, *91*, 4564−4566.
(16) Ou, C. C.; Wollmann, R. G.; Hendrickson, D. N.; Potenza, J. A.; Schugar, H. J. *J. Am. Chem. Soc.* **1978**, *100*, 4717−4724.
(17) Meagher, A. *Inorg. Chim. Acta* **1988**, *146*, 19−23.
(18) Pan, H. K.; Yarusso, D. J.; Knapp, G. S.; Pineri, M.; Meagher, A.; Coey, J. M. D.; Cooper, S. L. *J. Chem. Phys.* **1983**, *79*, 4736−4745.
(19) Lopes, L.; de Laat, J.; Legube, B. *Inorg. Chem.* **2002**, *41*, 2505−2517.
(20) Chatlas, J.; Jordan, R. B. *Inorg. Chem.* **1994**, *33*, 3817−3822.
(21) Morrison, T. I.; Shenoy, G. K.; Nielsen, L. *Inorg. Chem.* **1981**, *20*, 3565−3566.
(22) Morrison, T. I.; Reis, A. H.; Knapp, G. S.; Fradin, F. Y.; Chen, H.; Klippert, T. E. *J. Am. Chem. Soc.* **1978**, *100*, 3262−3264.
(23) Magini, M.; Saltelli, A.; Caminiti, R. *Inorg. Chem.* **1981**, *20*, 3564−3565.
(24) Khalid, S.; Caliebe, W.; Siddons, P.; So, I.; Clay, B.; Lenhard, T.; Hanson, J.; Wang, Q.; Frenkel, A. I.; Marinkovic, N.; Hould, N.; Ginder-Vogel, M.; Landrot, G. L.; Sparks, D. L.; Ganjoo, A. *Rev. Sci. Instrum.* **2010**, 81.
(25) Ravel, B.; Newville, M. *J. Synchrotron Radiat.* **2005**, *12*, 537−541.
(26) Webb, S. *Phys. Scr.* **2005**, *T115*, 1011−1014.
(27) Ankudinov, A. L.; Rehr, J. J. *Phys. Rev. B* **1997**, *56*, R1712−R1716.
(28) Mørup, S.; Knudsen, J. E.; Nielsen, M. K.; Trumpy, G. *J. Chem. Phys.* **1976**, *65*, 536−543.
(29) Becke, A. D. *J. Chem. Phys.* **1993**, *98*, 5648−5652.
(30) Lee, C.; Yang, W.; Parr, R. G. *Phys. Rev. B* **1988**, *37*, 785−789.
(31) Mcgrath, M. P.; Radom, L. *J. Chem. Phys.* **1991**, *94*, 511−516.
(32) Frisch, M. J. T., G. W.; Schlegel, H. B.; Scuseria, G. E.; Robb, M. A.; Cheeseman, J. R.; Montgomery, Jr., J. A.; Vreven, T.; Kudin, K. N.; Burant, J. C.; Millam, J. M.; Iyengar, S. S.; Tomasi, J.; Barone, V.; Mennucci, B.; Cossi, M.; Scalmani, G.; Rega, N.; Petersson, G. A.; Nakatsuji, H.; Hada, M.; Ehara, M.; Toyota, K.; Fukuda, R.; Hasegawa, J.; Ishida, M.; Nakajima, T.; Honda, Y.; Kitao, O.; Nakai, H.; Klene, M.; Li, X.; Knox, J. E.; Hratchian, H. P.; Cross, J. B.; Bakken, V.; Adamo, C.; Jaramillo, J.; Gomperts, R.; Stratmann, R. E.; Yazyev, O.; Austin, A. J.; Cammi, R.; Pomelli, C.; Ochterski, J. W.; Ayala, P. Y.; Morokuma, K.; Voth, G. A.; Salvador, P.; Dannenberg, J. J.; Zakrzewski, V. G.; Dapprich, S.; Daniels, A. D.; Strain, M. C.; Farkas, O.; Malick, D. K.; Rabuck, A. D.; Raghavachari, K.; Foresman, J. B.; Ortiz, J. V.; Cui, Q.; Baboul, A. G.; Clifford, S.; Cioslowski, J.; Stefanov, B. B.; Liu, G.; Liashenko, A.; Piskorz, P.; Komaromi, I.; Martin, R. L.; Fox, D. J.; Keith, T.; Al-Laham, M. A.; Peng, C. Y.;

Nanayakkara, A.; Challacombe, M.; Gill, P. M. W.; Johnson, B.; Chen, W.; Wong, M. W.; Gonzalez, C.; and Pople, J. A. *Gaussian 03*, Revision C.02. Gaussian Inc.: Wallingford, CT, 2004.
(33) Frisch, M. J. T., G. W.; Schlegel, H. B.; Scuseria, G. E.; Robb, M. A.; Cheeseman, J. R.; Scalmani, G.; Barone, V.; Mennucci, B.; Petersson, G. A.; Nakatsuji, H.; Caricato, M.; Li, X.; Hratchian, H. P.; Izmaylov, A. F.; Bloino, J.; Zheng, G.; Sonnenberg, J. L.; Hada, M.; Ehara, M.; Toyota, K.; Fukuda, R.; Hasegawa, J.; Ishida, M.; Nakajima, T.; Honda, Y.; Kitao, O.; Nakai, H.; Vreven, T.; Montgomery, Jr., J. A.; Peralta, J. E.; Ogliaro, F.; Bearpark, M.; Heyd, J. J.; Brothers, E.; Kudin, K. N.; Staroverov, V. N.; Kobayashi, R.; Normand, J.; Raghavachari, K.; Rendell, A.; Burant, J. C.; Iyengar, S. S.; Tomasi, J.; Cossi, M.; Rega, N.; Millam, N. J.; Klene, M.; Knox, J. E.; Cross, J. B.; Bakken, V.; Adamo, C.; Jaramillo, J.; Gomperts, R.; Stratmann, R. E.; Yazyev, O.; Austin, A. J.; Cammi, R.; Pomelli, C.; Ochterski, J. W.; Martin, R. L.; Morokuma, K.; Zakrzewski, V. G.; Voth, G. A.; Salvador, P.; Dannenberg, J. J.; Dapprich, S.; Daniels, A. D.; Farkas, Ö.; Foresman, J. B.; Ortiz, J. V.; Cioslowski, J.; Fox, D. J. *Gaussian 09*, Revision A.1; Gaussian Inc.: Wallingford, CT, 2009.
(34) Tomasi, J.; Mennucci, B.; Cances, E. *J. Mol. Struct.: THEOCHEM* **1999**, *464*, 211−226.
(35) Rossman, G. R. *Am. Mineral.* **1975**, *60*, 698−704.
(36) Scheinost, A. C.; Chavernas, A.; Barron, V.; Torrent, J. *Clay Clay Miner.* **1998**, *46*, 528−536.
(37) Zhu, M.; Legg, B.; Zhang, H.; Gilbert, B.; Ren, Y.; Banfield, J. F.; Waychunas, G. A. *Environ. Sci. Technol.* **2012**, *46*, 8140−8147.
(38) Sakane, H.; Munoz-Paez, A.; Diaz-Moreno, S.; Martinez, J. M.; Pappalardo, R. R.; Sanchez Marcos, E. *J. Am. Chem. Soc.* **1998**, *120*, 10397−10401.
(39) Miyanaga, T.; Sakane, H.; Watanabe, I. *Phys. Chem. Chem. Phys.* **2000**, *2*, 2361−2365.
(40) Munoz-Paez, A.; Pappalardo, R. R.; Sanchez Marcos, E. *J. Am. Chem. Soc.* **1995**, *117*, 11710−11720.
(41) Wang, J.; Rustad, J. R.; Casey, W. H. *Inorg. Chem.* **2007**, *46*, 2962−2964.
(42) Knudsen, J. M.; Larsen, E.; Moreira, J. E.; Nielsen, O. F. *Acta Chem. Scand. Ser. A* **1975**, *29*, 833−839.
(43) Mørup, S.; Knudsen, J. E. *Acta Chim. Hung.* **1986**, *121*, 147−171.
(44) Knudsen, J. E. *J. Phys. Chem. Solids* **1977**, *38*, 883−896.
(45) Koch, C. B.; Rasmussen, H. K.; Mørup, S. *Spectrochim Acta A* **2009**, *74*, 928−930.
(46) Jackson, W. G.; McGregor, B. C.; Jurisson, S. S. *Inorg. Chem.* **1987**, *26*, 1286−1291.
(47) Appleton, T. G.; Hall, J. R.; Ralph, S. F.; Thompson, C. S. M. *Inorg. Chem.* **1989**, *28*, 1989−1993.
(48) Richens, D. T. *The Chemistry of Aqua Ions: Synthesis, Structure and Reactivity: A Tour Through the Periodic Table of the Elements*; John Wiley & Sons Ltd: Chichester, U.K., 1997; pp 86−89.
(49) Crimp, S. J.; Spiccia, L.; Krouse, H. R.; Swaddle, T. W. *Inorg. Chem.* **1994**, *33*, 465−470.
(50) Stefansson, A. *Environ. Sci. Technol.* **2007**, *41*, 6117−6123.
(51) Milburn, R. M.; Vosburgh, W. C. *J. Am. Chem. Soc.* **1955**, *77*, 1352−1355.
(52) Sham, T. K. *Acc. Chem. Res.* **1986**, *19*, 99−104.
(53) Sham, T. K.; Hastings, J. B.; Perlman, M. L. *J. Am. Chem. Soc.* **1980**, *102*, 5904−5906.
(54) Herdman, G. J.; Neilson, G. W. *J. Phys.: Condens. Matter* **1992**, *4*, 627−638.
(55) Magini, M.; Caminiti, R. *J. Inorg. Nucl. Chem.* **1977**, *39*, 91−94.
(56) Pokrovski, G. S.; Schott, J.; Farges, F.; Hazemann, J.-L. *Geochim. Cosmochim. Acta* **2003**, *67*, 3559−3573.
(57) Reem, R. C.; McCormick, J. M.; Richardson, D. E.; Devlin, F. J.; Stephens, P. J.; Musselman, R. L.; Solomon, E. I. *J. Am. Chem. Soc.* **1989**, *111*, 4688−4704.
(58) Norman, R. E.; Holz, R. C.; Menage, S.; Que, L.; Zhang, J. H.; O'Connor, C. J. *Inorg. Chem.* **1990**, *29*, 4629−4637.
(59) Murray, K. S. *Coord. Chem. Rev.* **1974**, *12*, 1−35.
(60) Spiccia, L.; Stoeckli-Evans, H.; Marty, W.; Giovanoli, R. *Inorg. Chem.* **1987**, *26*, 474−482.
(61) Jolivet, J.-P.; Chaneac, C.; Tronc, E. *Chem. Commun.* **2004**, 477−483.